Article

Institution of MECHANICAL ENGINEERS

Journal of RAIL AND RAPID TRANSIT

Proc IMechE Part F:
J Rail and Rapid Transit
2022, Vol. 0(0) 1–12

DOI: 10.1177/09544097221141517
journals.sagepub.com/home/pif
SAGE

Application of yaw dampers with frequency-selective damping to improve the locomotive adaptability to low/high conicity stability

Guang Li[1], Yan Zhou[1], Yuan Yao[1], Xiaoyi Hu[2] and Ling Wei[3]

Abstract

High-speed locomotives are prone to the carbody or bogie hunting under extreme wheel-rail contact conditions, which can cause negative impacts on vehicle dynamics performance. The influence of key suspension parameters on the carbody lateral ride comfort and bogie lateral acceleration is investigated by the multi-objective optimization and Sobol global sensitivity analysis methods, which is based on the Radial Basis Function Neutral Network surrogate model. The results illustrate that the yaw damper damping is sensitive to the two hunting stabilities, but conventional yaw dampers with fixed damping fail to satisfy both the stability demands simultaneously. Therefore, this paper presents a damping-adjustable yaw damper integrating an FSD (frequency-selective damping) valve to guarantee the lateral stability especially in abnormal wheel-rail contact states, and the application effects of the FSD yaw damper for the locomotive are researched by dynamics simulations. The results show that the FSD yaw damper can improve the adaptability of the locomotive to both the low and high wheel-rail contact conicity service conditions compared with the conventional yaw dampers.

Keywords

High-speed locomotive, frequency-selective damping, lateral ride comfort, lateral stability, global sensitivity analysis, surrogate model

Date received: 9 July 2022; accepted: 25 October 2022

Introduction

In recent years, a certain type of domestic high-speed locomotive (B_0-B_0) often produces the carbody low-frequency swaying when the locomotive runs on some dedicated straight tracks in the state of new reprofiling wheel and new grinding rail profile, which makes drivers or passengers feel uncomfortable and attracts widespread attention of railway departments, and many scholars have conducted thorough investigations on this problem. The exiting researches found that the excessively polished rail in the gauge corner and larger rail cant could lead to an extremely low wheel-rail contact conicity, which may cause the carbody low-frequency swaying (primary instability) and deteriorate lateral ride comfort.[1–5] Then, several measures to alleviate the carbody hunting are put forward, including the tread repair and optimization of suspension parameters. Among them, reducing the yaw damper damping is one of the effective methods to improve lateral ride comfort, which has been verified by the on-track test.[6–8] However, the locomotive is prone to the bogie hunting (secondary instability) in the state of worn tread, which usually requires a larger yaw damper damping to guarantee the vehicle lateral stability.[9,10] Then essence of both two forms of hunting instability is that the lateral stability of railway vehicles equipped with passive suspension elements with stationary parameters is unqualified in a wide wheel-rail contact state considering lower and higher equivalent conicities.

The yaw damper, as one of the fundamental suspension components of railway vehicles, is installed longitudinally between the carbody and the frame, which can considerably suppress the carbody's yaw motion and attenuate the frame's lateral vibration, enhancing hunting critical speed. Therefore, a reasonable selection for yaw damper parameters is particularly noteworthy, which can improve lateral ride comfort and reduce the wheel-rail lateral force.[11–14] Yan et al.[15,16] deeply investigated the impact of the yaw damper's damping and series stiffness on the bogie stability and bifurcation type, and integrated the central popular

[1]State Key Laboratory of Traction Power, Southwest Jiaotong University, Chengdu, China
[2]Railway Science & Technology Research & Development Center, China Academy of Railway Sciences Corporation Limited, Beijing, China
[3]ITT High Precision Manufactured Products (Wuxi) Co., Ltd., Wuxi, China

Corresponding author:
Yuan Yao, State Key Laboratory of Traction Power, Southwest Jiaotong University, 111 2nd Ring Rd North Section 1, Jinniu District, Chengdu 610031, China.
Email: yyuan8848@163.com

theorem with the paradigm method to acquire the expressions for critical speed and bifurcation types, which were related to the damping and series stiffness of yaw dampers. Xia et al.[17] developed a bogie mechanical model with four degrees of freedom, and researched the impression of yaw damper's suspension parameters and installation position on lateral stability, ride comfort and steering ability. Besides, there are some researches about the accurate modeling of yaw dampers: Yang et al.[18] proposed to establish the piecewise linear model by considering the rubber joint stiffness, oil stiffness and piecewise characteristics of hydraulic dampers, and conducted the dynamics characteristic test for yaw dampers and compared test results with the traditional Maxwell model. The results showed that the piecewise linear model can accurately reflect the dynamics characteristic of yaw dampers. Alonso et al.[19] developed a simplified physical model for yaw dampers, which can guarantee accuracy without excessively increasing the computing time. In addition, the influence of yaw dampers on the vehicle's dynamics stability was analyzed, and it was demonstrated that the accurate modelling of yaw dampers is extremely important when predicting the dynamics behavior of railway vehicles.

Generally, hydraulic dampers are utilized as yaw dampers and the nominal damping is a constant value, which is difficult to meet the requirements of low and high conicity stabilities in the meantime, but the yaw damper with variable damping can perfectly handle the contradiction between low and high conicity stabilities. At present, researches on variable damping dampers mainly focus on magnetorheological dampers, which are utilized to improve the lateral ride comfort and hunting stability of railway vehicles.[20–23] However, the semi-active damper currently has some deficiencies in safety and real-time control, and passive dampers with some special structures can attain the function of variable damping without the above deficiencies. Based on the optimal dissipation theory and the Maxwell model for dampers, Yao et al.[24] derived the functional relationship between the damping and stiffness of the damper to achieve optimal dissipation, and the frequency-dependent stiffness of the yaw damper was proposed and applied to high-speed trains in the form of a simplified dynamics model, whose results showed that it can provide a better adaptability for the lateral stability of high-speed trains under different equivalent conicities. Huo et al.[25] developed a stiffness-adjustable yaw damper integrating an FSS (frequency-selective stiffness) valve and compared it with two conventional yaw dampers, and it was demonstrated that the FSS yaw damper can enhance the adaptability of railway vehicles to both low and high wheel-rail contact conicity conditions by numerical simulations and laboratory tests. Nevertheless, it should be noted that the premise is that the low and high conicity stabilities for railway vehicles are sensitive to the series stiffness of yaw dampers.

FSD damper model

Physical model of FSD damper

Since the inertial forces associated with the passive damper are minor and can be negligible, the force transmitted by dampers can be regarded as a velocity function. For traditional hydraulic dampers, when the cross-section area of the piston rod is equal to half of the pressure cylinder's cross-sectional area, the rebound force F_r and compressive force F_c produced by the damper with oil flow can be expressed as[26]

$$F_r = \frac{(A_1 - A_2)^3 \gamma}{2g\mu^2 {B_1}^2} v^2 \tag{1}$$

$$F_c = \frac{(A_1 - A_2)^3 \gamma}{2g\mu^2 {B_2}^2} v^2 + \frac{{A_2}^3 \gamma}{2g\mu^2 {B_3}^2} v^2 \tag{2}$$

In equations (1) and (2), A_1 and A_2 represent the cross section area of the piston and piston rod, respectively. B_1, B_2, and B_3 indicate the tensile orifice area, compression orifice area and bottom valve orifice area. γ stands for the density of liquids, and μ indicates the flow coefficient of orifices. In addition, v is the velocity of pistons, and g is the acceleration of gravity, 9.81 m/s^2.

Regarding the conventional damper, the value of A_2 is a constant, while A_2 is a variable value for the FSD damper (the damper of frequency-selective damping), whose essence is that the FSD characteristic of the FSD damper is achieved by changing the value of A_2 with the variation of excitation frequency. The sectional view of the FSD damper is shown in Figure 1(a), and the damping force is mainly originated from four sets of valves arranged on the piston, which includes two sets of rebound and compression valves. Compared with traditional hydraulic dampers, the FSD damper has one set of frequency valves,[27] which contain rebound and compression valves, and the switch of the frequency valve can be controlled to change the cross section area of orifices, thus altering the damping value of the FSD damper. Also, the corresponding frequency value for the switching of frequency valve is regarded as the cut-off frequency of the FSD damper.

The detailed working procedure of the frequency valve is described in Figure 1(b), which can be divided into three stages including closed state, open process and open state. When the motion frequency of pistons is high, the oil cannot flow from the constant orifice to the first auxiliary chamber within a short period, and the piston motion enters the next half-cycle, so the auxiliary piston remains closed. At this time, the frequency valve is in a closed state, resulting in a large damping value for the FSD damper. Then, with the decrease of the motion frequency for pistons, the oil in the second auxiliary chamber has enough time to flow into the first auxiliary chamber through the constant orifice, whose flow direction is indicated by arrow 8 in the figure, but the frequency valve is still closed, which causes the damper to show a large damping state as well. Besides, when the frequency valve is fully open, the oil in the rebound chamber flows to the compression chamber through the first auxiliary chamber, whose flow directions are implied by arrows 9 and 10, and the FSD damper exhibits a small damping state.

Mathematical model of FSD damper

According to the FSD characteristic for the FSD damper and the Maxwell model,[28,29] the mathematical model of the FSD damper is established in MATLAB/SIMULINK, as shown in Figure 2. In order to make the damper model exhibit low and high damping states for excitations at low

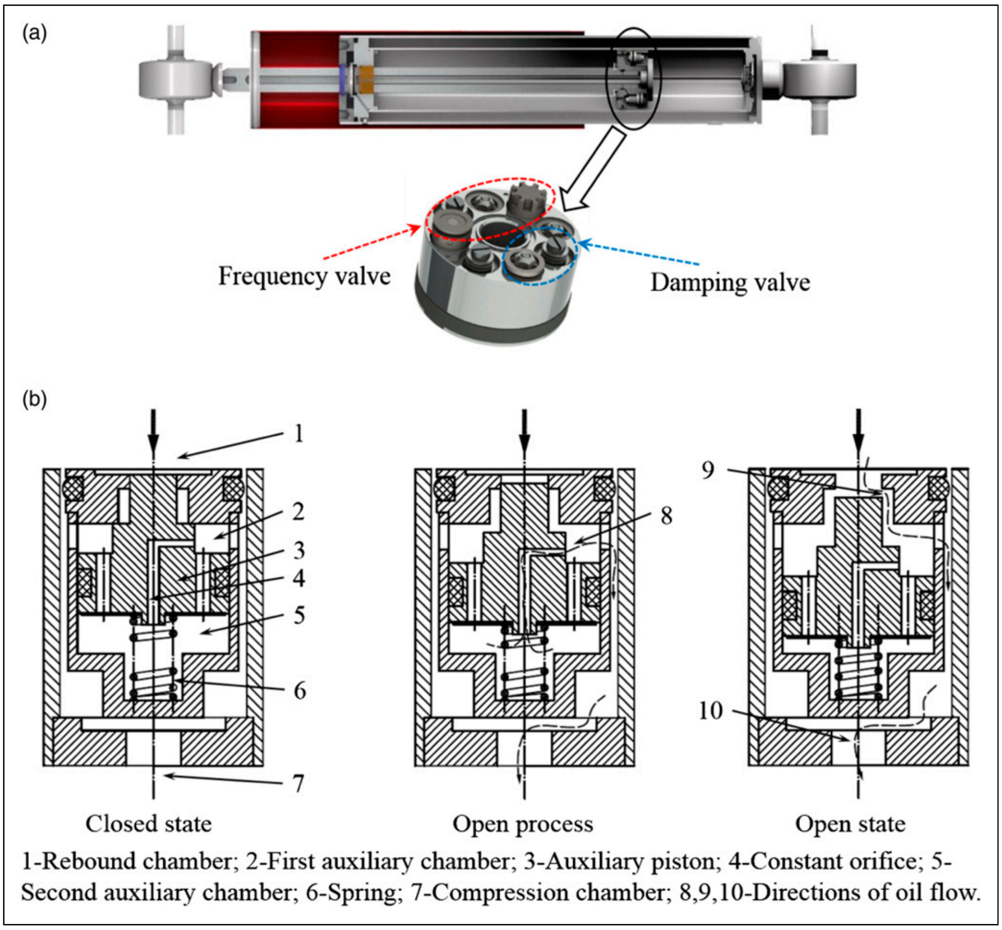

Figure 1. The sectional view of the Frequency-Selective Damping (FSD) damper and the working procedure of frequency valve.

and high frequencies, the model is composed of four modules, which include the low/high damping module, the frequency valve module, the trigger module and the scale factor module. Besides, the opening process of frequency valves requires a certain time, which is equivalent to the time delay effect and is considered in the model, and the main parameters of the FSD damper model are shown in Appendix Table A1.

FSD damper simulation

In order to verify the FSD characteristic of the developed FSD damper model, the hysteretic curve of the FSD damper is analyzed and compared with those in relation to 2 conventional dampers, and 2 sine excitations with different frequencies of 1 Hz and 4 Hz are considered. In addition, Figure 3 illustrates the force-velocity curves of the 3 damper models, including 2 conventional dampers and the FSD damper, and their damping values are 200 kN.s/m, 800 kN.s/m and 200 & 800 kN.s/m (200 kN.s/m at low frequency excitation, 800 kN.s/m at high frequency excitation), which are represented with symbols YD1, YD2 and FSD. It is worth noting that the damping values of FSD dampers at low/high frequency excitation are equal to the damping values of YD1 and YD2 dampers.

Figure 4 shows the comparison of hysteretic curves for the above mentioned dampers, where the horizontal axis stands for the piston displacement, and the vertical axis represents the damper force. Figures 4(a)–(c) are hysteretic curves of the three dampers under 1 Hz sine excitation, which are corresponded to YD1, YD2 and FSD dampers respectively, and Figures 4(d)–(f) are hysteretic curves of the three dampers under 4 Hz sine excitation. It can be found from the figure that under 1 Hz sine excitation, the hysteretic curve of the FSD damper is close to that of the YD1 damper, which indicates that the FSD damper shows a small damping state. However, when the dampers are under 4 Hz sine excitation, the FSD damper shows the basically same hysteretic curves as the YD2 damper, which represents that the FSD damper exhibits a large damping state at this time. The above results reveal that the FSD damper can achieve the feature of FSD, whose specific behavior is to exhibit a small damping state for low frequency excitation and a large damping state for high frequency excitation. Besides, there are "teeth" shapes in Figure 4(c), which is because the FSD damper will show a certain oscillation when the frequency valve is open.

Locomotive simulation model and condition

Locomotive dynamics model

In terms of the structure and suspension parameters for a certain type of high-speed locomotive with B_0-B_0 axle

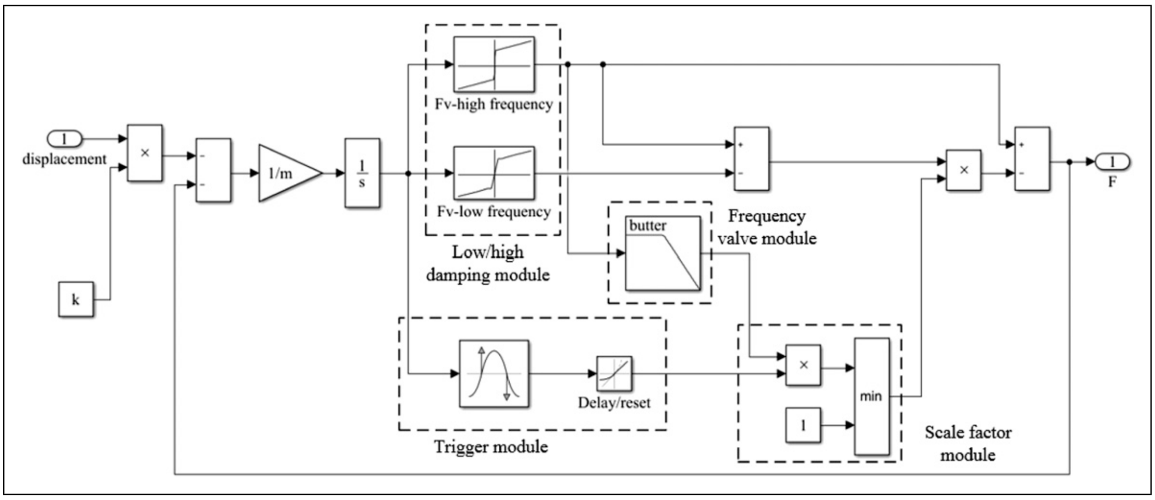

Figure 2. The mathematical model of the FSD damper.

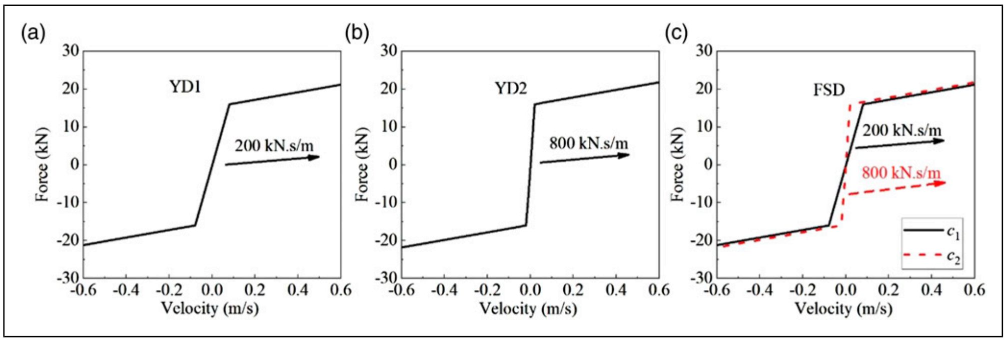

Figure 3. Force versus velocity curves of three dampers (YD1, YD2 and FSD).

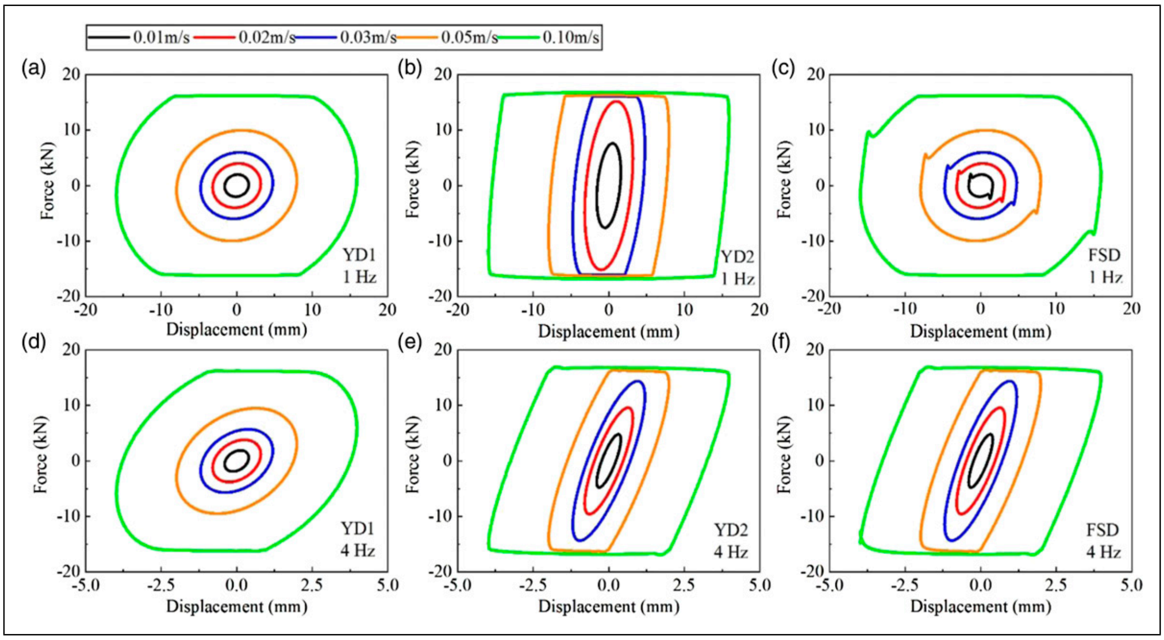

Figure 4. Hysteretic curves for the three dampers.

arrangement in China, the corresponding vehicle dynamics model is established by the commercial software SIMPACK, as shown in Figure 5(a). The specific parameters for the model are shown in Appendix Table A2. The locomotive dynamics model consists of 25 rigid bodies, which contain one carbody, 2 frames, 4 wheelsets, 4 motors, 4 hollow shafts, 2 traction rods and eight rotary arms of axle box. Among them, the function of the hollow shaft is to transfer power from the motor to the drive shaft of the wheelset. Furthermore, several bodies own 6 degrees of freedom (DOFs) in space, which involve the carbody, frame, wheelset and motor, and each hollow shaft holds three DOFs relative to the wheelset, including lateral, yaw and roll motions. In addition, every traction rod allows pitch and yaw DOFs along to the carbody, and each rotary arm possesses only one DOF to rotate around the wheelset axle, so the locomotive dynamics model has a total of 90 DOFs. Besides, the wheel-rail contact is constructed based on the CN60 rail and JM3 profiles, and the track gauge is set to 1.435 m. Moreover, the wheel-rail tangential force is computed through the FASTSIM algorithm,[30,31] where the value of Kalker coefficient is set to 1, and the elastic contact ellipse properties are approximated employing an equivalent-elastic contact search procedure in SIMPACK.

There are many suspension elements in the bogie suspension system, which can be classified into two major categories: primary suspension and secondary suspension.[32,33] Concretely, the primary suspension performs between the frame and the wheelset, whose lateral and longitudinal stiffness are afforded by the positioning of rotary arms, and the primary vertical stiffness is provided by the primary axle box spring. The secondary suspension acts between the carbody and the frame, which is mainly composed of secondary lateral, yaw and vertical dampers as well as high round springs, and secondary lateral stops are also considered. All the damper elements are built based on the Maxwell model concerning spring and damper in series. In addition, the Wuguang High-speed Rail measured track irregularity[34–36] is chosen as the track excitation in next time-domain simulations, and the accuracy of the established locomotive dynamics model has been verified through on-track test results.[37]

As depicted in Figures 5(a) and (b), Mote Carlo simulations based on the Latin Hypercube sampling method are implemented by the MATLAB/SIMPACK co-simulation platform, whose function is to accomplish the global sensitivity analysis and multi-objective optimization for suspension parameters, and the data exchange is done through SIMPACK scripting language '.sjs' and '.qs'. For the intention of analyzing the influence of FSD yaw dampers on the locomotive lateral dynamics performance, we can substitute the elements of conventional yaw dampers in the dynamics model with the mathematical model of FSD yaw dampers, which is achieved through the SIMPACK/SIMULINK co-simulation interface, see Figures 5(a) and (c). Specifically, the two software systems are calculated at the same time, and the real-time data exchange between the mathematical model of FSD yaw dampers and the locomotive dynamics model is realized by the interface module SIMAT. Besides, the two systems independently adopt their own solvers to calculate and exchange data at the time node set by the program.

Simulation condition

The wheel-rail contact equivalent conicity is a very important dynamics index for railway vehicles, which will seriously affect lateral dynamics performance. Therefore, with respect to the high-speed locomotive using the original yaw damper YD2, vehicle dynamics behaviors on straight tracks with different JM3 tread states are studied, including the thin flange, new wheel and worn wheel states. The three profiles of JM3 tread and the corresponding equivalent conicity curves are shown in Figure 6, and the values of the nominal equivalent conicity are 0.04, 0.10 and 0.7, which are regarded as three different operational scenarios (S_{low}, S_{norm} and S_{high}), corresponding to the low-conicity, normal-conicity and high-conicity conditions, respectively. In the dynamics simulation for the locomotive running on straight tracks with the above prescribed operational scenarios, the carbody lateral ride comfort index W_y and the bogie lateral acceleration A_{yb} are extracted,[38,39] and the calculation equation of W_y is described as[40–42]

$$W_y = 3.57 \sqrt[10]{\frac{A_{yc}^3}{f} F(f)} \tag{3}$$

Where A_{yc} represents the amplitude in the frequency domain derived from an FFT analysis of the measured carbody

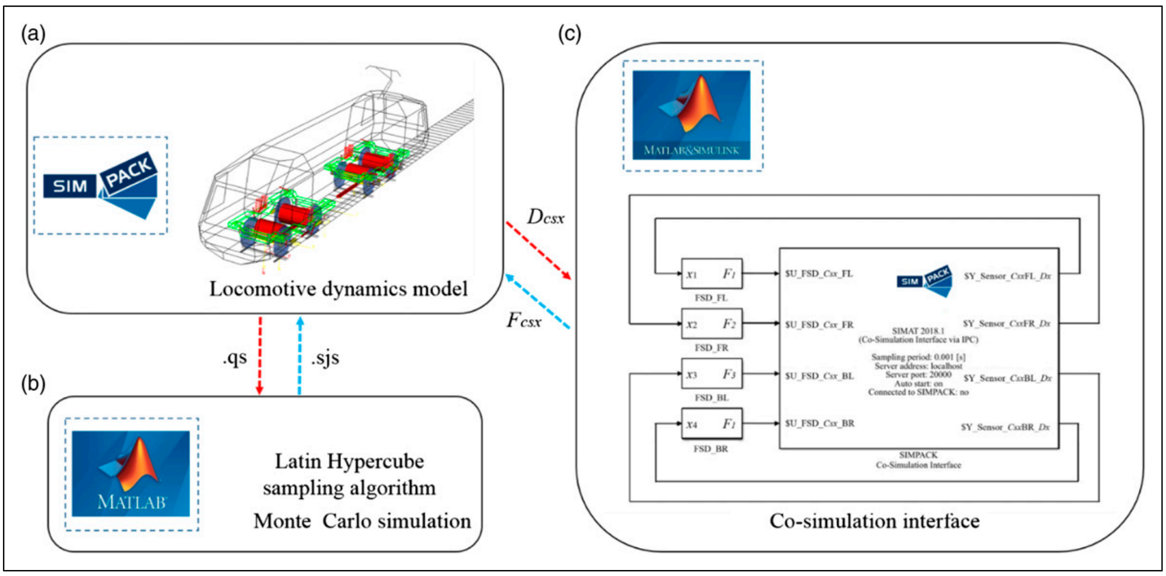

Figure 5. Locomotive dynamics model and simulation process.

lateral acceleration, and f stands for the corresponding frequency. $F(f)$ indicates the frequency correction coefficient, which can be obtained through searching the frequency correction coefficient table from GB/T5599-2019. Moreover, when the value of W_y is less than 2.75, the locomotive lateral ride comfort is regarded as an excellent level, and a smaller value of W_y indicates a better lateral ride comfort performance for railway vehicles. Besides, it should be noted that the measurement position of carbody lateral acceleration A_{yc} is usually located at the carbody floor when calculating the value of W_y.

In Figures 7(a) and (b), the horizontal axis represents the vehicle running speed, and the ordinate axes indicate the W_y and A_{yb}, respectively. With the increase of running speeds, the values of carbody lateral ride comfort index W_y and bogie lateral acceleration A_{yb} continue to be augmented. During the lower speed ranges, the values of W_y and A_{yb} are smaller, which indicates that the carbody lateral ride comfort and bogie lateral stability are better. When the running speed is higher, the carbody lateral ride comfort is poor for the S_{low} condition and the statistical value of bogie lateral acceleration A_{yb} is the largest for the S_{high} condition, which reflects that the carbody and bogie hunting are prone to occur under low and high conicity conditions, respectively. Also, the locomotive lateral dynamics performance in the S_{norm} condition is always between the other two conditions. Therefore, the S_{low} and S_{high} conditions are selected to investigate the effect of FSD dampers on locomotive's running performance under straight tracks, and the running speed is set to 200 km/h. Besides, we can conclude that the carbody lateral ride comfort index W_y for the S_{low} condition can

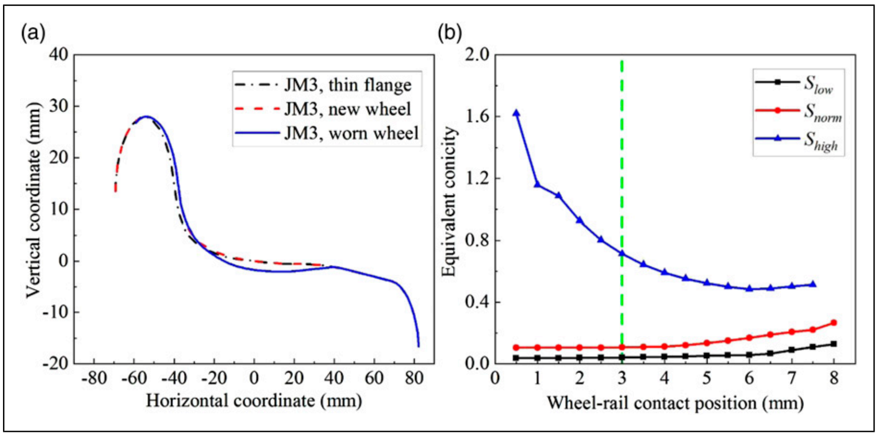

Figure 6. The three profiles of JM3 tread and equivalent conicity curves.

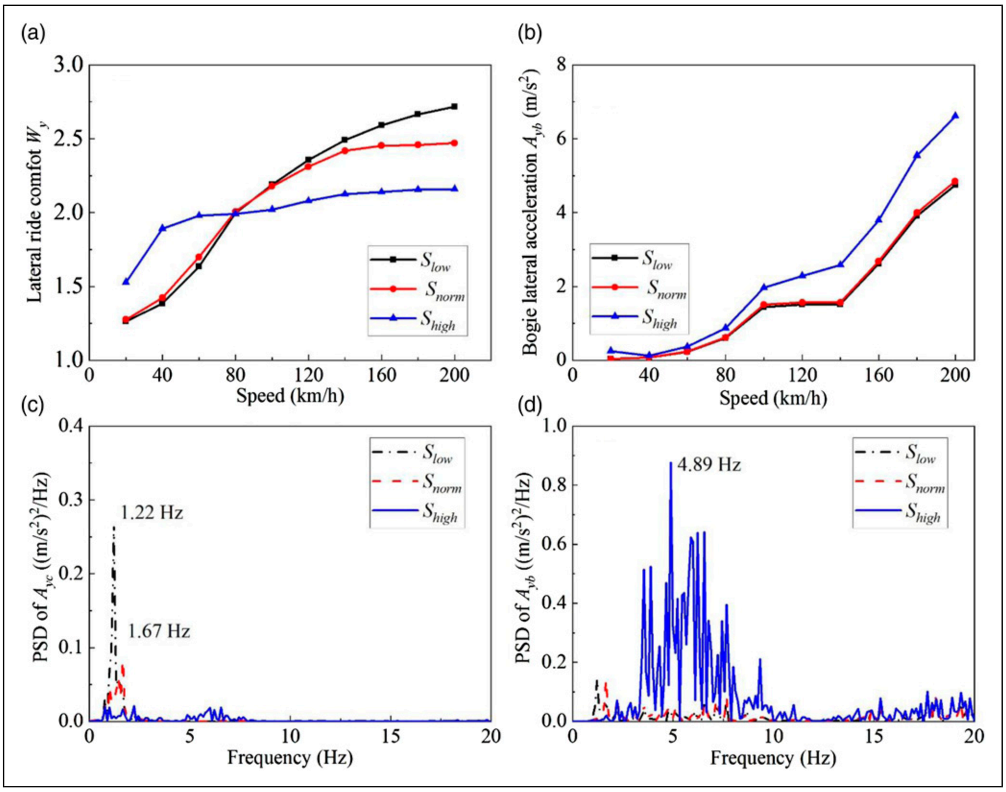

Figure 7. Simulation results of W_y and A_{yb} and PSD results of A_{yc} and A_{yb} for different conditions.

Table 1. Design parameters and optimization ranges.

Parameter	Design range	Description
K_{px}	10~50 (kN/mm)	Primary longitudinal stiffness
K_{py}	2~10 (kN/mm)	Primary lateral stiffness
C_{sx}	200~1200 (kN.s/m)	Damping of yaw damper
C_{sy}	10~60 (kN.s/m)	Damping of secondary lateral damper
K_{ncsx}	10~50 (kN/mm)	Series stiffness of yaw damper
K_{ncsy}	10~50 (kN/mm)	Series stiffness of secondary lateral damper

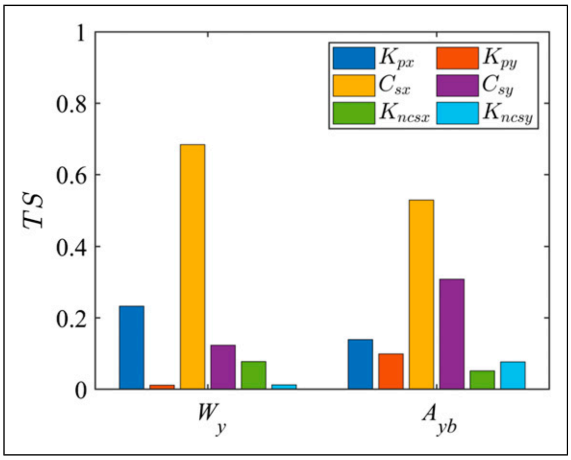

Figure 8. Global sensitivity analysis results.

imply the low conicity stability, and the bogie lateral acceleration A_{yb} for the S_{high} condition can represent the high conicity stability.

In order to deeply analyze the frequency distribution of lateral ride comfort and bogie lateral acceleration, the spectrum analysis[43] is performed on the carbody lateral acceleration A_{yc} and the bogie lateral acceleration A_{yb} in the above three conditions, where the running speed is 200 km/h, and the analysis results are shown in Figures 7(c) and (d). It can be drawn that the vibration energy of A_{yc} in the S_{low} condition is the maximum, and the dominant frequency of A_{yc} is around 1.22 Hz. Besides, the vibration energy of A_{yb} in the S_{high} condition is the maximum, and the dominant frequency of A_{yb} is around 4.89 Hz. Accordingly, in order to make the FSD yaw damper show different damping states for low and high conicity conditions, it is reasonable to set the cut-off frequency of the FSD yaw damper to 2 Hz.

Suspension parameter analysis and optimization

Global sensitivity analysis

Global sensitivity analysis (GSA) can help to discover how important design parameters are, and how to reduce the number of design parameters. Usually, global sensitivity analysis methods contain the FAST method, OAT method and Morris method, etc.[44] The Sobol sensitivity analysis method[45] is used here, and its important aspects involve examining sensitivity from the standpoint of variance decomposition, as well as quantifying input and output uncertainty in the form of the probability distribution. Furthermore, the advantages of this method include the ability to analyze interaction and nonlinear response, as well as robust and trustworthy sensitivity analysis results.

This section intends to conduct GSA between low/high conicity stability and several key suspension parameters, including the primary longitudinal stiffness K_{px}, the primary lateral stiffness K_{py}, the damping of yaw damper C_{sx} and the series stiffness of yaw damper K_{ncsx}, as well as the secondary lateral damper damping C_{sy} and its series stiffness K_{ncsy}. Furthermore, the lateral ride comfort index W_y for the S_{low} condition and the bogie lateral acceleration A_{yb} for the S_{high} condition are obtained from the time-domain simulation results in SIMPACK software, and the two indexes are utilized to represent the low and high conicity stabilities, respectively. In order to obtain more accurate sensitivity analysis results and simultaneously improve computational efficiency, the random sampling of parameters is carried out through Monte Carlo simulations based on the Latin Hypercube Sampling (LHS) method.[46] The sampling number of LHS is set to 200, and sampling ranges for the above six suspension parameters are described in Table 1. Besides, the vehicle operating speed and distance are set to 200 km/h and 500 m in all time-domain simulations below. The total sensitivity index TS is adopted as the evaluation index here, and the sensitivity analysis results are shown in Figure 8. The horizontal axis represents the two optimization objectives, which correspond lateral ride comfort index W_y and bogie lateral acceleration A_{yb}. The vertical axis indicates the total sensitivity index TS, and the larger value of TS stands for the corresponding sensitivity is stronger. It can be drawn that W_y and A_{yb} are sensitive to K_{px}, C_{sx} and C_{sy}, but insensitive to K_{py}, K_{ncsx} and K_{ncsy}. Namely, when the values of K_{px}, C_{sx} and C_{sy} fluctuate, the carbody lateral ride comfort and bogie lateral stability change significantly, but the variation in K_{py}, K_{ncsx} and K_{ncsy} values has little influence on the two optimization objectives. Besides, it should be noted that the two objectives are both most sensitive to the value of C_{sx}.

Surrogate model and multi-objective optimization

Common surrogate models include Kriging and Neural Network as well as Response Surface surrogate models, etc. Among them, the Radial Basis Function Neutral Network (RBFNN) surrogate model possesses excellent approximation ability and faster learning speed, which is widely utilized in many practical engineering fields. The structural characteristics for the RBFNN surrogate model[47] are shown in Figure 9, where the model is a three-layer feedforward network composed of input layers, single hidden layers and output layers. Specifically, the input layer imports m input

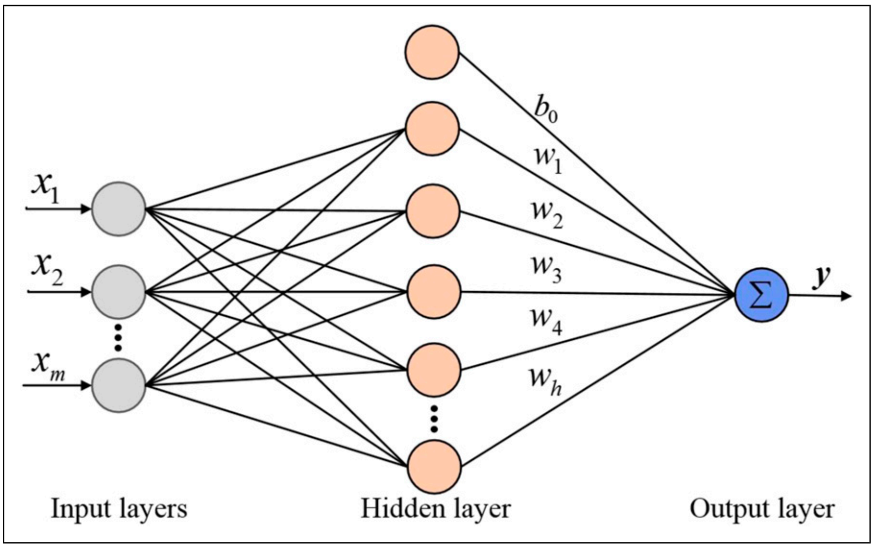

Figure 9. The schematic diagram of RBFNN surrogate model.

parameters into the model in the form of a vector $\boldsymbol{x} = [x_1, x_2, \ldots, x_m]^T$, which is nonlinearly transformed by the hidden layer neurons, and then linearly transformed by the output layer. Finally, the output vector $\boldsymbol{y} = [y_1, y_2, \ldots, y_n]^T$ consisting of n responses is obtained.

In theory, RBFNN has the ability to approximate arbitrarily complex nonlinear mappings, which can be described as

$$f = \boldsymbol{R}^m \rightarrow \boldsymbol{R}^n \quad (4)$$

By definition, the output response is calculated as

$$\boldsymbol{y} = f(\boldsymbol{x}) = \sum_{i=1}^{h} w_i \phi(\|\boldsymbol{x} - \boldsymbol{u}_i\|) + b_0 \quad (5)$$

In equation (5), $\boldsymbol{x} \in \boldsymbol{R}^m$, $\boldsymbol{y} \in \boldsymbol{R}^n$. H is the number of neurons in the hidden layer, and $\boldsymbol{u_i}$ is the center vector of the hidden node in the hidden layer, $\boldsymbol{u}_i \in \boldsymbol{R}^m$. b_0 represents the bias value, and w_i indicates the weighting coefficient. $\|\cdot\|$ stands for the European Biridian norm, and $\phi(\cdot)$ implies a Gaussian radial basis function.

Affected by the local characteristics of the radial basis function, if the $\boldsymbol{x}$ is farther away from the $\boldsymbol{u_i}$, the lower the activation degree of the neuron, and the worse the model fitting ability. Therefore, by introducing the K-means clustering algorithm, the surrogate model self-organizes to select $\boldsymbol{u_i}$ from the input vector, and dynamically adjusts the activation degree of neurons.

Then, to assure the accuracy of the constructed RBFNN surrogate model, the decision coefficient R^2 is given as follows

$$R^2 = 1 - \frac{\sum_{i=1}^{n} \left(y_i - \hat{y}_i\right)^2}{\sum_{i=1}^{n} \left(y_i - \bar{y}_i\right)^2} \quad (6)$$

Where n stands for the number of test samples, y_i ($i = 1,2, \ldots, n$) donates the test value of the test sample, and $\hat{y}_i$ represents the results calculated by the surrogate model. The value of R^2 is between 0 and 1, and the closer the value of R^2 is to 1, the better the global approximation of the surrogate model.

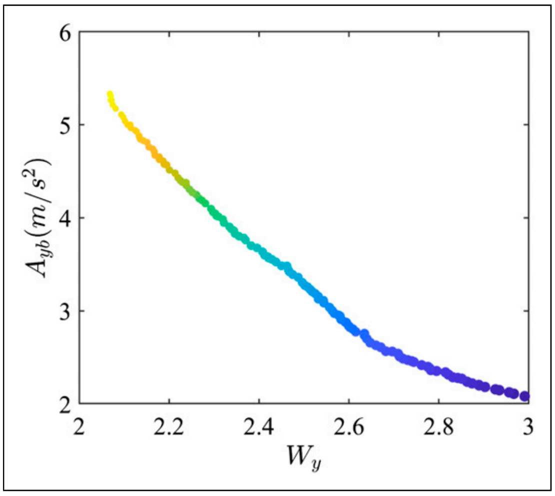

Figure 10. Pareto frontier for the optimization.

Based on the above Monte Carlo simulation results, a RBFNN surrogate model is established through the above mentioned theory, where the number of neurons is 10. The decision coefficient R^2 for the constructed surrogate model is greater than 0.9, which means that the model fits well and has higher accuracy. Experience shows that when $R^2 > 0.8$, the surrogate model can forecast the value that fulfills the accuracy standards and meets the demands of optimizing the design parameters.[48] Then, the constructed surrogate model is utilized to conduct the multi-objective optimization, which is because surrogate models have the advantage of fast calculation. The optimization objectives and design parameters are the same as the Monte Carlo simulation, and the optimization trend is to obtain smaller values of W_y and A_{yb}. The genetic algorithm NSGA-II is utilized as the optimization algorithm to solve the multi-objective optimization problem, and the population size and the number of iterations are set to 500 and 100, respectively. Besides, the default setting for other parameters are preserved.

Figure 10 shows the Pareto frontier for the multi-objective optimization, and the abscissa and vertical axes represent the lateral ride comfort index W_y and bogie lateral acceleration A_{yb}. The colour for the data point indicates the value of A_{yb}, and the darker the colour, the smaller the value of A_{yb}, which means the vehicle has a better high conicity stability. It can be drawn from the figure that there is a strong contradiction between W_y and A_{yb}, which implies that the low conicity stability and high conicity stability are conflicting. When the high-speed locomotive has good lateral ride comfort of the carbody, the vibration for the bogie frame is generally severe under the high conicity condition. On the contrary, when the bogie lateral stability for the locomotive is good, the carbody lateral ride comfort under the low conicity condition is poor. Therefore, we should take into account the two dynamics performances simultaneously according to the actual requirements when designing the suspension parameters.

The Pareto sets regarding W_y are depicted in Figure 11. The vertical axis of each subgraph stands for an optimized suspension parameter, and the colour depth of the data point represents the value of A_{yb} as well. It can be concluded that decreasing the damping of yaw dampers and secondary lateral dampers is beneficial to improving the carbody lateral ride comfort under the low conicity condition, but unfavorable for the bogie lateral stability under the high conicity condition. In addition, the optimization results show that the value of K_{px} is concentrated in 10~14 kN/mm. The distribution for the remaining three optimized parameters does not show obvious laws. Besides, it is worth noting that both W_y and A_{yb} are highly sensitive to C_{sx}, so this paper proposes to investigate the adaptability of the FSD yaw damper to lateral dynamics performance for the locomotive under low and high wheel-rail contact conicity conditions.

Influence of FSD yaw damper on locomotive dynamic performance

Since the above researches show that the demands of low and high conicity stabilities against the yaw damper damping are contradictory and have strong sensitivity, this section analyzes the adaptability of the yaw damper with FSD to the low and high conicity stabilities, which is based on the SIMPACK/SIMULINK co-simulation. The influence of FSD yaw dampers on lateral dynamics performance is studied when the locomotive runs on straight tracks with the S_{low} and S_{high} conditions, and compared with the above mentioned two conventional yaw dampers: YD1 and YD2. The carbody lateral acceleration A_{yc} for the S_{low} condition and the bogie lateral acceleration A_{yb} for the S_{high} condition are extracted to evaluate the corresponding lateral stability.

Figures 12(a) and (b) illustrate the carbody and bogie lateral acceleration responses obtained through dynamics simulation, and the abscissa axis represents the simulation time. Usually, a smaller yaw damper damping is beneficial to improving the carbody ride comfort, while a larger yaw damper damping can strength coupling impact between the carbody and bogie motions, which is conductive to suppressing lateral vibration of bogies. It can be concluded from the figure that when the locomotive adopts the YD1 yaw damper, the amplitude of the carbody lateral acceleration A_{yc} is small, but the amplitude of the bogie lateral acceleration A_{yb} is large. On the contrary, when the YD2 yaw damper is employed, the amplitude of A_{yb} is small, while the amplitude of A_{yc} is large. The above results show that the selection of yaw dampers with the fixed damping value needs to compromise the contradiction between the low and high conicity stabilities, so it is difficult to ensure vehicle lateral stability in extreme wheel-rail contact conditions. For the locomotive with the FSD yaw damper, the amplitude of both A_{yc} and A_{yb} are smaller, which indicates that the FSD yaw damper can guarantee the low and high conicity stabilities simultaneously.

Figures 12(c) and (d) show the power spectral density results of carbody lateral acceleration A_{yc} and bogie lateral acceleration A_{yb}, and the dominant frequency for A_{yc} and A_{yb} are around 1.22 Hz and 4.89 Hz respectively. Specifically,

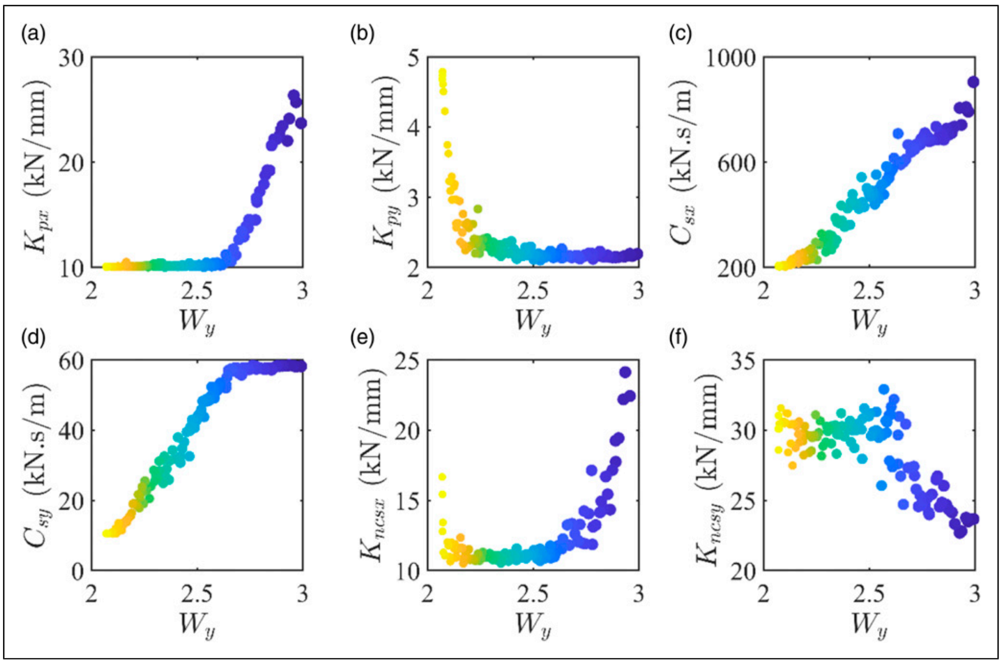

Figure 11. The distribution of design parameters regarding W_y of Pareto frontier.

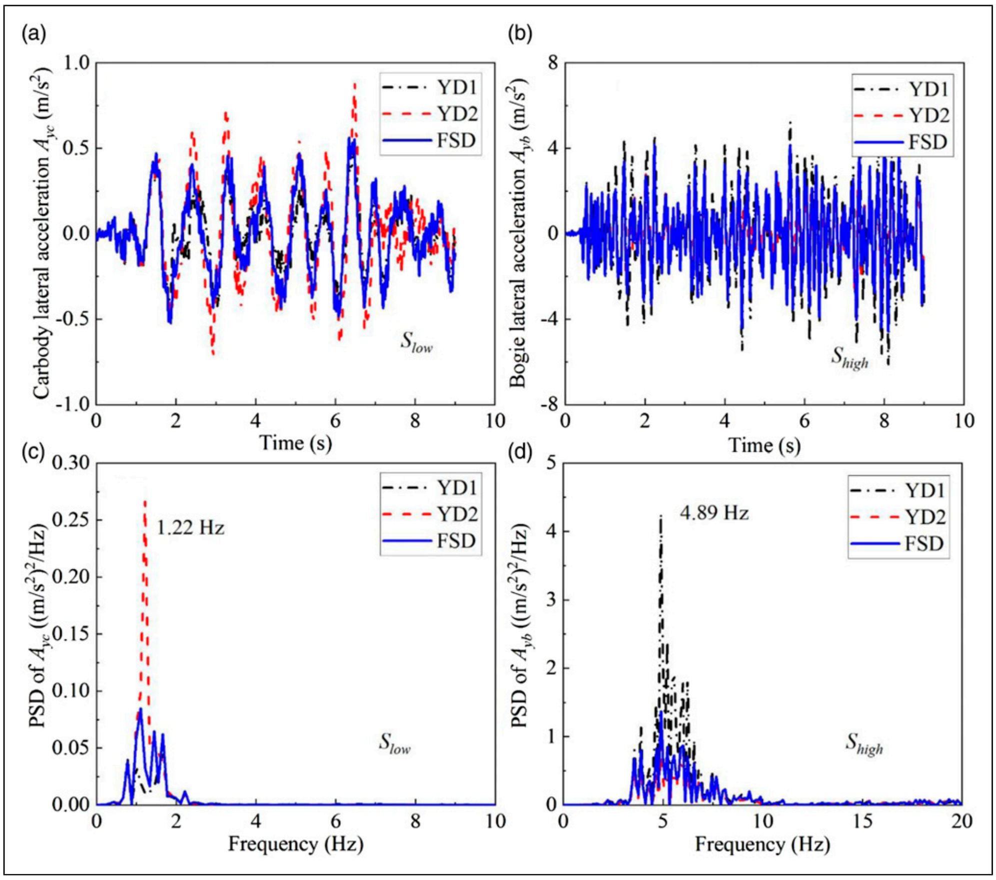

Figure 12. The simulation results of A_{yc} and A_{yb} and their PSD results.

when the locomotive utilizes the YD1, YD2 and FSD yaw dampers, respectively, the peak values of the dominant frequency corresponding to A_{yc} are successively 0.02, 0.27 and 0.03, and the peak values of the dominant frequency corresponding to A_{yb} are 4.26, 0.88 and 1.37 in turn, where the unit is '$(m/s^2)^2$/Hz'. It can be concluded that the vibration energy of A_{yc} in its dominant frequency with the YD2 yaw damper is maximum, which is prone to the carbody low-frequency swaying, and the vibration energy of A_{yb} in its dominant frequency with the YD1 yaw damper is utmost, resulting in the bogie hunting easily. The FSD yaw damper can reduce the vibration energy of A_{yc} for the S_{low} condition and A_{yb} for the S_{high} condition, and achieve a better adaptability to the straight tracks with both low and high conicity conditions in comparison with the other two conventional yaw dampers.

Conclusions

(1) This paper proposes a damping-adjustable yaw damper integrating an FSD valve to improve the adaptability of the locomotive to low and high conicity stabilities, which can achieve a FSD feature. Moreover, the corresponding mathematical model is established in MATLAB/SIMULINK, and the simulation analysis is conducted to verify the feature of FSD. The results reveal that the FSD damper model can exhibit a small damping state under low frequency excitation, while a large damping state under high frequency excitation.

(2) Global sensitivity analysis between six key suspension parameters and low/high conicity stability is implemented, which is based on the Monte Carlo simulation using the Latin hypercube sampling, and the multi-objective optimization is conducted regarding the constructed RBFNN surrogate model. The results show that both low and high conicity stabilities are sensitive to the damping of yaw dampers, and a small damping of yaw damper can improve the low conicity stability, while a large damping of yaw damper is required for the high concitiy condition. Conventional yaw dampers with fixed damping has the shortcoming of not guaranteeing the lateral stability of railway vehicles under abnormal wheel-rail contact conicity conditions.

(3) The application effects of the FSD yaw damper for the high-speed locomotive are investigated, including the straight tracks with low and high conicity conditions. The results demonstrate that compared with the two conventional yaw dampers, the FSD yaw damper can improve lateral ride comfort for the low conicity condition and simultaneously ensure the bogie lateral stability for the high conicity condition.

The above research conclusions are obtained based on the dynamics software's simulation analysis results, which can only provide a certain theoretical support for the application of FSD yaw dampers. Overall, compared with traditional measures to settle low and high conicity stabilities instability, the FSD yaw damper can provide a better lateral stability adaptability to extreme wheel-rail contact states, which is also a more economic approach. Besides, the presentation of FSD yaw dampers adapts to the development tread of intelligent components, and will play an increasingly important role in the future. However, if the FSD yaw damper will be installed on the actual running railway vehicles, it is still necessary to conduct a large number of experimental studies on the FSD yaw damper, including component tests and vehicle bench tests.

Acknowledgements

The authors are grateful to the anonymous reviewers for providing insightful comments aimed at improving the paper.

Declaration of conflicting interests

The author(s) declared no potential conflicts of interest with respect to the research, authorship, and/or publication of this article.

Funding

The author(s) disclosed receipt of the following financial support for the research, authorship, and/or publication of this article: The material in this paper is based on work supported by grants from the National Railway Group Science and Technology Program grant (N2020J026, N2021J028), and Traction Power State Key Laboratory grant (2022TPL_Q02) of the Independent Research and Development Projects.

ORCID iD

Guang Li https://orcid.org/0000-0002-3190-0357

References

1. Cooperrider NK. The hunting behavior of conventional railway trucks. *J Eng Ind* 1972; 94: 752–761.
2. Garg VK and Dukkipati RV. *Dynamics of railway vehicle system*. New York: Academic Press, 1984.
3. Wickens AH. Static and dynamic instabilities of bogie railway vehicles with linkage steered wheelsets. *Veh Sys Dyn* 1996; 26: 1–16.
4. Lee SY and Cheng YC. Hunting stability analysis of high-speed railway vehicle trucks on tangent tracks. *J Sound Vib* 2005; 282: 881–898.
5. Iwnicki S. *Handbook of railway vehicle dynamics*. Boca Raton: CRC Taylor & Francis, 2006.
6. Huang CH, Zeng J and Liang SL. Carbody hunting investigation of a high speed passenger car. *J Mech Sci Technol* 2013; 27: 2283–2292.
7. Bideleh SMM, Berbyuk V and Persson R. Wear/comfort Pareto optimisation of bogie suspension. *Veh Syst Dyn* 2016; 54: 1053–1076.
8. Sun JF, Chi MR, Jin XS, et al. Experimental and numerical study on carbody hunting of electric locomotive induced by low wheel-rail contact conicity. *Veh Syst Dyn* 2021; 59: 203–223.
9. Fujimoto H and Miyamoto M. Lateral vibration and its decreasing measure of a Shinkansen train. *Veh Syst Dyn* 1996; 25: 188–199.
10. Wei L, Zeng J, Chi MR, et al. Carbody elastic vibrations of high-speed vehicles caused by bogie hunting instability. *Veh Syst Dyn* 2017; 55: 1321–1342.
11. Persson R, Andersson E, Stichel S, et al. Bogies towards higher speed on existing tracks. *Int J Rail Transp* 2014; 2: 40–49.
12. Zhang H, Ran XR, Wang XG, et al. Coupling effects of yaw damper and wheel-rail contact on ride quality of railway vehicle. *Shock Vib* 2021. DOI: 10.1155/2021/6692451.
13. Wang WL, Huang Y, Yang XJ, et al. Non-linear parametric modelling of a high-speed rail hydraulic yaw damper with series clearance and stiffness. *Nonlinear Dyn* 2011; 65: 13–34.
14. Wang WL, Yu DS, Huang Y, et al. A locomotive's dynamic response to in-service parameter variations of its hydraulic yaw damper. *Nonlinear Dyn* 2014; 77: 1485–1502.
15. Yan Y, Zeng J, Huang CH, et al. Bifurcation analysis of railway bogie with yaw damper. *Arch Appl Mech* 2019; 89: 1185–1199.
16. Yan Y and Zeng J. Hopf bifurcation analysis of railway bogie. *Nonlinear Dyn* 2018; 92: 107–117.
17. Xia ZH, Zhou JS, Gong D, et al. Theoretical study on the effect of the anti-yaw damper for rail vehicles. *Proc Inst Mech Eng C-J Mec* 2019; 234: 457–473.
18. Yang DX, Chi MR, Cai WB, et al. Study on piecewise linear model of anti-yaw damper and test analysis. In: Proceedings of the 2015 International Industrial Informatics and Computer Engineering Conference. Xi'an, China, 2015.
19. Alonso A, Giménez JG and Gomez E. Yaw damper modelling and its influence on railway dynamic stability. *Veh Syst Dyn* 2011; 49: 1367–1387.
20. Wang DH and Liao WH. Semi-active suspension systems for railway vehicles using magnetorheological dampers. Part II: simulation and analysis. *Veh Syst Dyn* 2009; 47: 1439–1471.
21. Shin YJ, You WH, Hur HM, et al. Semi-active control to reduce carbody vibration of railway vehicle by using scaled roller rig. *J Mech Sci Technol* 2012; 26: 3423–3431.
22. Zong LH, Gong XL, Xuan SH, et al. Semi-active H∞ control of high-speed railway vehicle suspension with magnetorheological dampers. *Veh Syst Dyn* 2013; 51: 600–626.

23. Kim HC, Shin YJ, You W, et al. A ride quality evaluation of a semi-active railway vehicle suspension system with MR damper: railway field tests. *Proc Inst Mech Eng Part F J Rail Rapid Transit* 2017; 231: 306–316.
24. Yao Y, Chen XW, Li H, et al. Suspension parameters design for robust and adaptive lateral stability of high-speed train. *Veh Syst Dyn* 2022. DOI: 10.1080/00423114.2022.2062012.
25. Huo WB, Yue BS, Liu XG, et al. The development of stiffness-adjustable anti-yaw damper. In: Proceeding of the the IAVSD International Symposium on Dynamics of Vehicles on Roads and Tracks. Gothenburg, Sweden, 2019.
26. Yang GZ. *Hydraulic damper for rolling stocks*. Beijing: China Railway Publishing House, 2003.
27. Decock P. *Fluid-filled frequency dependent damper*. Patent 201280054137-ZH, China, 2014.
28. Yao Y, Li G, Wu GS, et al. Suspension parameters optimum of high-speed train bogie for hunting stability robustness. *Int J Rail Transp* 2019; 8: 195–214.
29. Chen XW, Yao Y, Shen LJ, et al. Multi-objective optimization of high-speed train suspension parameters for improving hunting stability. *Int J Rail Transp* 2022; 10: 159–176.
30. Kalker JJ. A fast algorithm for the simplified theory of rolling contact. *Veh Syst Dyn* 1982; 11: 1–13.
31. Iwnicki S. Simulation of wheel–rail contact forces. *Fatigue Fract Eng M* 2003; 26: 887–900.
32. True H and Asmund R. The dynamics of a railway freight wagon wheelset with dry friction damping. *Veh Sys Dyn* 2003; 38: 149–163.
33. Bruni S, Vinolas J, Berg M, et al. Modelling of suspension components in a rail vehicle dynamics context. *Veh Sys Dyn* 2011; 49: 1021–1072.
34. Li JY, Liu LY and Kou DH. Wu Guang high-speed rail track irregularity power spectrum analysis. *Appl Mech Mater* 2014; 638: 1224–1228.
35. Zhai WM, Han ZL, Chen ZW, et al. Train-track-bridge dynamic interaction: a state-of-the-art review. *Veh Syst Dyn* 2019; 57: 984–1027.
36. Cheng F, Wei K, Zhao ZM, et al. Track dynamic geometry state prediction for straight/curved low-stiffness urban rail transit viaduct lines based on virtual track inspection method. *Veh Syst Dyn* 2021. DOI: 10.1080/00423114.2021.2007956.
37. Li G, Wu RD, Deng XX, et al. Suspension parameters matching of high-speed locomotive based on stability/comfort Pareto optimization. *Veh Syst Dyn* 2021. DOI: 10.1080/00423114.2021.1979602.
38. Polach O. On non-linear methods of bogie stability assessment using computer simulations. *Proc Inst Mech Eng Part F: J Rail Rapid Transit* 2006; 220: 13–27.
39. Polach O. Characteristic parameters of nonlinear wheel/rail contact geometry. *Veh Sys Dyn* 2010; 48: 19–36.
40. Suzuki H. Research trends on riding comfort evaluation in Japan. *Proc Inst Meche Eng Part F J Rail Rapid Transit* 1998; 212: 61–72.
41. Kim YG, Kwon HB, Kim SW, et al. Correlation of ride comfort evaluation methods for railway vehicles. *Proc Inst Meche Eng Part F J Rail Rapid Transit* 2003; 217: 73–88.
42. National Railway Administration, GB/T5599. *Specification for dynamic performance assessment and testing verification of rolling stock*. China, Beijing: National Railway Administration, 2019. (in Chinese).
43. Zhai WM, Liu PF, Lin JH, et al. Experimental investigation on vibration behaviour of a CRH train at speed of 350 km/h. *Int J Rail Transp* 2015; 3: 1–16.
44. Iooss B and Lemaître P. *A review on global sensitivity analysis methods, uncertainty management in simulation-optimization of complex systems*. US: Springer, 2015.
45. Nossent J, Elsen P and Bauwens W. Sobol' sensitivity analysis of a complex environmental model. *Environ Modell Softw* 2011; 26: 1515–1525.
46. Kassa E and Nielsen JCO. Stochastic analysis of dynamic interaction between train and railway turnout. *Veh Syst Dyn* 2008; 46: 429–449.
47. Khairy E and Chris L. Robust parameter design optimization using kriging, RBF and RBFNN with gradient-based and evolutionary optimization techniques. *Appl Math Comput* 2014; 236: 325–344.
48. You TW, Gong D, Zhou JS, et al. Frequency response function-based model updating of flexible vehicle body using experiment modal parameter. *Veh Syst Dyn* 2021. DOI: 10.1080/00423114.2021.1983182.

Appendix

Table A1. Main parameters of the frequency-selective damping damper model.

Item	Value	Unit
Equivalent damping (low frequency) c_1	200	kN.s/m
Equivalent damping (high frequency) c_2	800	kN.s/m
Equivalent mass m	15	Kg
Equivalent stiffness k	15	kN/mm
Cut-off frequency of frequency valve f_p	2	Hz
Switching delay of frequency valve t	0.05	S

Table A2. Locomotive model parameters.

Item	Value	Unit
Carbody mass	42e3	kg
Bogie frame mass	3441	kg
Wheelset mass	2434	kg
Wheel base	2.9e3	mm
Length between bogie centres	9e3	mm
Distance of contact point	1493	mm
Wheel rolling radius	625	mm
Friction coefficient	0.3	/
Rail cant	1:40	/
Primary vertical stiffness	15	kN/mm
Primary longitudinal stiffness	15	kN/mm
Primary lateral stiffness	3.5	kN/mm
Damping of secondary lateral damper	25	kN.s/m
Series stiffness of secondary lateral damper	25	kN/mm
Damping of yaw damper	800	kN.s/m
Series stiffness of yaw damper	22.5	kN/mm